*Robotica* (2022), **40**, pp. 4498–4511
doi:10.1017/S0263574722001060

CAMBRIDGE UNIVERSITY PRESS

RESEARCH ARTICLE

# Energy-aware redundant actuation for safe spring-assisted modular and reconfigurable robot

Christopher Singh and Guangjun Liu*

Department of Aerospace Engineering, Toronto Metropolitan University, 350 Victoria St., Toronto, Ontario M5B 2K3, Canada
*Corresponding author. E-mail: gjliu@ryerson.ca

**Received:** 3 April 2022; **Revised:** 21 June 2022; **Accepted:** 27 June 2022; **First published online:** 1 August 2022

**Keywords:** actuation and joint mechanisms, cellular and modular robots, energy-aware automation, multiple working mode control, robot safety

## Abstract

A spring-assisted modular and reconfigurable robot (SA-MRR) has been recently developed at our laboratory to reinforce its performance and enable safe and dexterous operation in human–robot environments. Multiple working mode (MWM) control enables each SA-MRR joint module to switch independently between working in a primary actuation mode and a secondary, spring-assisted mode that may improve task-specific energy performance measures and safety in a variety of manipulation tasks. The spring-assisted mode is characterized by synergy of spring and motor energy and may be summoned to offset motor energy demands or to safeguard a reconfigurable set of secondary joint limits. In this research work, two spring-assisted working mode strategies are proposed, and their characteristics have been investigated for SA-MRR actuation energy advantages while safe robot segregation in collaboration tasks is maintained. One MWM strategy has been designed to safeguard task-specific joint limits and is able to decrease motor energy consumption in some tasks. Another MWM strategy has been designed for energy efficiency and was able to reduce motor energy per cycle by 72% in a simulated manipulation task while maintaining spatial safety constraints. Numerical simulations have demonstrated the effectiveness of the proposed spring-assisted working mode strategies for energy-aware safe manipulation applications.

## 1. Introduction

Modular and reconfigurable robots (MRRs) can be used in a wide variety of applications due to their versatility, flexibility, and adaptability. Preserving their competitive edge on contemporary application frontiers and in human environments (e.g., fixed base or mobile collaboration) necessitates higher safety and lower energy consumption. The challenge is to deliver both decisively, without compromising reconfigurability or performance.

Toward extending safe and efficient utility prospects of MRR manipulators, we have equipped several joint modules with a secondary mechanical operating mode (the *spring-assisted* mode) that serves to augment joint torque on an as-needed basis. This is another example of multiple working mode (MWM) actuation approaches under development at our laboratory. Recently, we applied online, active–passive MWM actuation methods successfully in sophisticated manipulation tasks [1, 2, 3]. For our spring-assisted MRR (SA-MRR), the secondary mechanical operating mode features a synergistic integration of MWM online control with the joint brake and the embedded spring [4]. Mechanically, this multiple-mode, hybrid active–passive redundant actuation scheme [5] belongs to the growing family of clutched parallel elastic actuation (CPEA) systems, cf. [6]. In this work, we propose applying MWM actuation methods for the first time to the spring-assisted MRR for heightened spatial manipulation safety and to reduce task-specific energy consumption.

A "task" could be any action or manipulation that a robot is assigned to do. Tasks may range from whole autonomous jobs to simple motion segments. In this research, our proposed MWM methods use energy awareness to apply the SA-MRR to known and chiefly repetitive tasks. In general, any elastic actuation method which does this optimally must consider nonlinear kinematics and dynamics of the robotic system in addition to loading characteristics of the task itself. Under known, cyclic robot trajectory and force requirements (i.e., a "task"), a global energy-optimal parallel-spring characteristic exists, as ref. [7] conclusively confirmed, but is generally nonlinear and is often discontinuous and difficult or impractical to realize for arbitrary tasks. Pioneering efforts to generalize elastic actuator metrics are underway by Calanca and Verstraten [8] who defined an energy efficiency index analytically. But their method [8] takes into account only resonance motions, and so it has yet to be shown how this energy metric may influence the design of parallel elastic actuation (PEA) systems for general robotics applications. For these reasons, our methods and most contemporary methods in recent literature are system-specific and rely on task-by-task analysis. Extensive research has been reported on (C)PEA, exploiting the available design variables to minimize actuator effort in either torque or energy [7, 9, 10, 11, 12, 13, 14, 15, 16, 17]. Several methods have been developed which harness PEA design parameters to holistically reshape the natural system dynamics toward meeting the overall energy requirements of cyclic tasks more closely (e.g., [10, 18]). Research has been reported to suit PEA for more general applications by considering a probabilistic distribution of tasks [19]. Some research includes modifying the tasks or motion trajectories themselves to exploit system resonance and to avail more design variables to have greater potential for actuation benefits (e.g., [9, 20]). Realistic pursuits to make PEA more suitable for manipulators have precipitated reports of standalone actuator development [11, 12], cam mechanisms, or controlled compliance adaptation with auxiliary actuators to realize nonlinear elastic behaviors [13, 14, 15], and numerous CPEA design variations for discontinuous spring torque delivery, and for freedom over spring energy storage, maintenance, and release [6, 12, 16]. In summary, task-specific energy is a driving concern of ours and other (C)PEA methods. But the primary intent and novelty of our proposed MWM methods is manipulation safety. Accordingly, our proposed MWM methods use the available design variables firstly to satisfy spatial safety constraints without modifying the task. Then, any remaining freedom in the design variables is harnessed to decrease actuation input energy for safety-critical tasks.

To the best of our knowledge, no other researchers have reported on (C)PEA methods for spatial manipulation safety. In ref. [21], Brown concludes that permanently connected parallel springs in articulated robot joints have no effect on *collision* safety. But before any collision, a violation of spatial segregation has occurred first. By a novel method presented in this paper, the SA-MRR helps to ensure segregation more decisively in shared workspaces by mechanically safeguarding task-specific joint limits. Each active SA-MRR manipulator joint delivers passive mechanical safeguarding over a pair of reconfigurable motion limits, within the range of the mechanical end stops. This is done via antagonism with the clutched parallel spring, in addition to software limits. By contrast to our SA-MRR, active robots are not typically designed with online reconfigurable, physically safeguarded joint motion limits. Bowyer et al. [22, Sec. VI-G] surveyed prominent passive collaboration and manipulation devices whose joints feature combinations of actuated, passive mechanical elements (dampers, brakes, and clutches, or continuously variable transmissions) used to enforce desired joint motion ratios or virtual limits passively, to "steer" the end-effector in path following and obstacle avoidance routines. It is well known that parallel elastic elements may reduce working ranges of robot joints. But PEA joint designs nearly always feature springs whose elastic characteristics specifically avoid counteracting the task (e.g., [18, 19]). Similarly, clutched PEA robot joints with at least two functional modes, cf. [6], typically avoid engaging parallel elastic elements whenever doing so would needlessly counteract the task (e.g., [23, 24]). Meanwhile, research by Niehues et al. [25] was found even to suggest exploiting actuator saturation for limiting the joint range of motion of their tendon-driven robotic finger with permanently connected parallel compliance elements. The underlying fact is unrefuted that parallel springs may provide actuation torque and energy benefits [7, 9, 10, 11, 12, 13, 14, 15, 16, 17], whereas the potential benefits of CPEA for safety are not commonly found in the literature.

Strength of the MWM method resides in adding spring features to the primary joint actuator in harmony with task-specific intent. Therefore, the challenge was to capitalize on the spring-assisted mode

https://doi.org/10.1017/S0263574722001060 Published online by Cambridge University Press

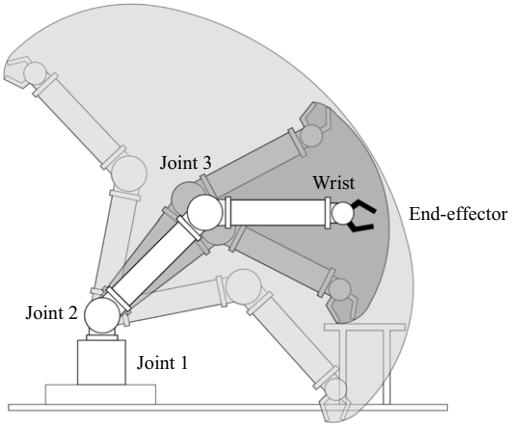


***Figure 1.*** *Illustration of 3-DoF SA-MRR regional structure with spring-assisted waist, shoulder, and elbow joints (planar slice shown). The SA-MRR keeps to its appointed territory (darker shading) in the task space by safeguarding rotation angle limits in the joint space. This makes more workspace available (lighter shading) for collaboration.*

by designing modular MWM strategies which improve MRR safety and reduce energy consumption. Accordingly, in this work we have developed two MWM strategies from the existing actuation capabilities: one energy-aware method for safety, followed by a safety-aware method that decreases motor energy consumption.

The first strategy emulates joint limiting that is safeguarded internally by a repelling spring torque on approach to the task-specific limit angles. This manipulation safety method ensures the SA-MRR keeps to its task-specific joint limits and is a novel CPEA application concept, Fig. 1.

The second spring-assisted strategy saves energy in repetitive tasks in known, confined workspaces with spring torque complementing the actuation effort. The work related most closely to this energy-saving MWM strategy is that by Brown and Ulsoy [26], who proposed retrofitting active manipulator joints with energy-minimizing parallel springs permanently connected. Distinctly, the SA-MRR joint module design enables online reconfiguration to initialize and adapt to known task variations by resetting the spring rest angle. Accordingly, in our step to identify the spring characteristic we search directly for the optimal spring rest angle that satisfies the additional task-specific safety constraints. Comparably, Brown and Ulsoy [19] find their energy-minimizing method to provide energy consumption savings between 60% and 80% in simulation for a 3-DoF manipulator arm.

In this work, both of the two developed SA-MRR actuation strategies are presented to address MRR energy consumption and safety for known, and chiefly repetitive tasks. The energy properties of both of the proposed MWM strategies are analyzed and then demonstrated through a numerical example.

The rest of this paper is organized as follows: Section 2 describes the SA-MRR system and modeling and elaborates the SA-MRR approach to task safety. Designs and energy properties are developed and analyzed in Section 3 for the two proposed MWM strategies. Simulation results in Section 4 demonstrate the energy characteristics of the two MWM actuation strategies. Conclusions follow in Section 5.

## 2. Spring-assisted MRR

### *2.1. Basic operating principle*

Design and motivation behind our spring-assisted MRR, including control framework based on joint torque sensing, was reported previously by Liu et al. [4]. Each SA-MRR joint module constitutes a clutched PEA system (Fig. 2) with two mechanical operating modes: (*Mode 1*), "moving-freely mode," and (*Mode 2*), "spring-connected mode" by convention [6]. Instead of immobilizing the module, activating the electromechanical brake engages the embedded flat spiral torsion spring in parallel with

https://doi.org/10.1017/S0263574722001060 Published online by Cambridge University Press

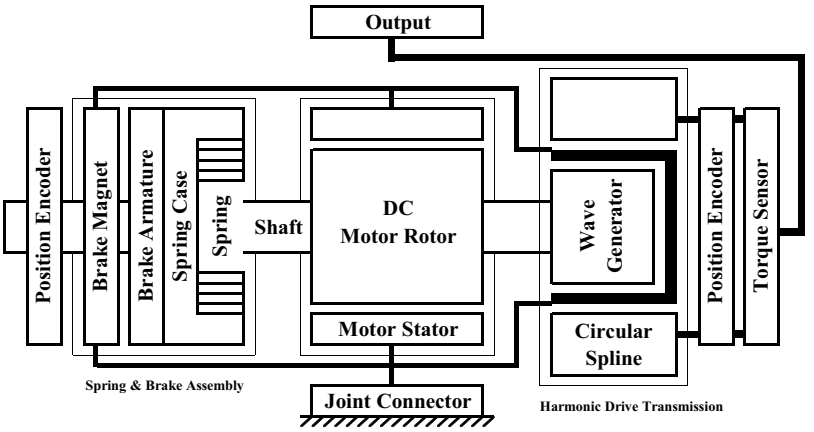


***Figure 2.*** *Schematic diagram of SA-MRR joint module. For true joint module section views and actual photographs, the reader is referred to [4].*

the DC motor shaft and transitions the SA-MRR module from (*Mode 1*) to (*Mode 2*). Deactivating the brake disengages the spring and transitions the module from (*Mode 2*) to (*Mode 1*). The mechanical components unique to the spring-assisted MRR module contribute less than 1% additional weight compared with our conventional MRR modules. Accordingly, added weight is not a significant concern when considering the energy consumption of SA-MRR modules.

### *2.2. Hybrid active–passive redundant actuation*

Engaging the spring in parallel creates a hybrid active–passive redundant actuation scenario where the spring contributes to actuation torque and energy delivery. Springs are passive mechanical elements that may only recycle prestored energy and cannot arbitrarily incite actuation energy. For each joint operating in (*Mode 2*), spring-assisted mode, torque and stored energy of the embedded spring are position-dependent and proportional to the joint displacement angle and to its square, respectively. Behind each MWM intent is the understanding that spring torque $\tau_k$ is equally capable of assisting or resisting instantaneous motor torque $\tau_m$. As such, each MWM strategy must generally be integrated into preplanned tasks. Meanwhile, (*Mode 1*) may comply globally with power-and-force limitations, as well with human–robot collaboration safety constraints for comprehensive SA-MRR safety in human environments.

### *2.3. SA-MRR system modeling*

The spring at joint module $i$, $(i = 1, \ldots, n)$ co-operates in actuator space. In (*Mode 1*), joint torque $\tau_i$ and motor torque $\tau_{m_i}$ are related through the speed reducer ratio $\gamma_i > 1$

$$\tau_{m_i} = \frac{\tau_i}{\gamma_i}. \tag{1}$$

Connecting the spring thus augments the required motor torque

$$\tau'_{m_i} = \frac{\tau_i}{\gamma_i} - \tau_{k_i} \tag{2}$$

https://doi.org/10.1017/S0263574722001060 Published online by Cambridge University Press

with spring torque, where prime notation denotes (*Mode 2*) operation. At module $i$, spring torque $\tau_{k_i}$ depends firstly on the operating mode defined by the brake state $b_i \in \mathbb{B}$

$$\tau_{k_i} = \begin{cases} \tau_{k_i}(\theta), & \text{brake engaged, } b_i = 1 \\ 0, & \text{brake disengaged, } b_i = 0 \end{cases} \tag{3}$$

and secondly on its torque–deflection characteristic as a function of the spring deflection angle $\theta$. Linear torsion springs with rest angle $\theta_0$ and positive stiffness $k_s$

$$\tau_{k_i}(\theta) = -k_{s_i}\Delta\theta_i = -k_{s_i}\left(\theta_i - \theta_{0_i}\right) \tag{4}$$

are assumed for modeling the spring features. Subscripts $i$ are often dropped hereafter for readability.

The $n$-DoF serial SA-MRR manipulator dynamics

$$M(q)\ddot{q} + C(q,\dot{q})\dot{q} + g(q) = \tau \tag{5}$$

has desired redundantly actuated torque $\tau$ expressed

$$\tau = \gamma(\tau_m' + \tau_k) \tag{6}$$

where $\gamma = \text{diag}(\gamma_1, \ldots, \gamma_n)$. No spring augmentation design strategy of one joint affects any other SA-MRR module.

### 2.4. SA-MRR energy consumption measures

Design, optimization, and evaluation of each of the two energy-aware MWM strategies rely integrally on the following two energy consumption measures for the SA-MRR joint modules:

1. **The *(Mode 1)* motor energy.** This is the active motor energy consumed per cycle by the desired repetitive task motion. It is also the initial motor energy expended on startup to set the spring connection angle:

$$E_m = \int P_m(t)\mathrm{d}t = \int_{t_0}^{t_1} \left( \frac{\tau_m(t)^2 R_m}{k_\tau^2} + |\gamma\tau_m(t)\dot{q}(t)| \right) \mathrm{d}t \tag{7}$$

   on $t = [t_0, t_1]$, where $P_m$, $R_m$, $k_\tau$ are the motor power, terminal resistance, and torque constant, respectively.

2. **The *(Mode 2)* motor energy.** This is the active motor energy consumed per cycle while the spring is connected:

$$E_m' = \int P_m'(t)\mathrm{d}t = \int_{t_0}^{t_1} \left( \frac{\tau_m'(t)^2 R_m}{k_\tau^2} + \left|\gamma\tau_m'(t)\dot{q}(t)\right| \right) \mathrm{d}t \tag{8}$$

   where the variables common to (7) are the same as above.

These two measures, (7), (8), are also used to report simulation results in Section 4 to quantify energy effectiveness of both of the two proposed MWM strategies.

### 2.5. SA-MRR system operating assumptions

Every MWM method changes task-specific motor demands and SA-MRR module operating conditions. While complementary methods lessen the motor load, antagonistic methods add spring torque and may nearly overload the motor. In this work, we assume a simplified DC motor model with linear relation between torque and current throughout its entire operating range, including at a suitably high torque threshold $|\tau_{m_{\max}}|$ that is very near but sufficiently less than the stall torque. We also assume symmetry $|\tau_{m_{\max}}| = |-\tau_{m_{\max}}|$ and motor ability to operate perhaps near-continuously around this threshold without performance degradation or heat damage.

https://doi.org/10.1017/S0263574722001060 Published online by Cambridge University Press

While spring stiffness $k_s$ is selected during design and is constant, it is fully reconfigurable offline through component swapping. For all SA-MRR operations in this research work, we assume the spring has no hysteretic effects, that it engages always from its undeflected equilibrium angle and that it influences the motor in no way besides its torque contribution. For the antagonistic method, the brake is required to operate during collaboration scenarios when the joint velocities are relatively lower, and we assume each joint brake changes state instantaneously with no position error.

### *2.6. SA-MRR segregation as primary safety intent*

Segregation is unequivocally the highest, most reliable form of robot safety. Spatial segregation is upheld intuitively for collaborators when robots keep within an appointed territory. State-of-the-art robot safety may allow humans and robots within mutual reach, but under highly regulated conditions that often compromise task efficiency. Instead, the SA-MRR may allow uninterrupted robot operation by spatially segregating its reach from humans [28]. The SA-MRR safety technique we develop in this work begins by already knowing a task-specific set of joint angle extrema (endpoints) that have been chosen independently for segregation safety and should be safeguarded. Also in this research work, the SA-MRR collaboration intent is that of humans and robots performing separate tasks in relatively close proximity, and with relatively lower robot velocities, but not of hands-on-robot or direct physical interactions. The workspace of the robot is limited by the ranges of the joint springs, leaving more workspace for humans.

## 3. Proposed MWM strategies

Benefits of the MWM method for energy-aware safety are obtained by harmonizing the spring features and the primary joint actuator demands with the task-specific intent. Accordingly, design and analysis of the following two proposed MWM strategies begins from offline $n$-DoF inverse dynamics of the task-specific manipulator trajectory and loading. This produces $n$ torque–angle relations in actuator space that forms the basis of our understanding to augment SA-MRR motor torque with spring torque. Visually, the torque–angle profile may be the source to identify safe task limits $\theta_{\min} < \theta_{\max}$ and may also affirm ultimate (in)feasibility of each task-specific MWM design strategy output by comparing $\tau'_m(\theta)$ to the motor limit $\pm|\tau_{m_{\max}}|$. While the design and analysis takes place in the torque–angle domain, the energy characteristics are known only from the time domain, (7), (8). To analyze the following two MWM strategies and their energy characteristics, quintic polynomial motion trajectories in actuator space with zero acceleration at endpoints have been considered.

### *3.1. Spring assistance to safeguard endpoints*

The first MWM strategy uses the spring to help achieve decisive, mechanical segregation of the robot arm and end-effector from the collaborators by safeguarding task-specific joint limits. While a spring is not a limiting device, we propose that a spring may be paired with a suitable task to resemble joint limiting with added safeguarding by the following rationale and method. If the available motor torque can be critically diminished using the spring, then the task endpoints may be held statically but not easily surpassed. Only retreat motion from the endpoints is possible in this static sense, and the approach toward endpoints is buffered safely by the spring. Thus, spatial segregation is achieved by mechanical limitation in addition to the task-specific software joint limits. However, not every task may allow for SA-MRR joint limit safeguarding, as described hereafter.

To implement this torque-based endpoint limiting strategy, the augmented motor torque $\tau'_m(\theta)$ at each joint shall satisfy

$$\tau'_m(\theta_{\min}) = -|\tau_{m_{\max}}|, \tag{9}$$

$$\tau'_m(\theta_{\max}) = +|\tau_{m_{\max}}|, \tag{10}$$

and act progressively via spring torque antagonism.

https://doi.org/10.1017/S0263574722001060 Published online by Cambridge University Press

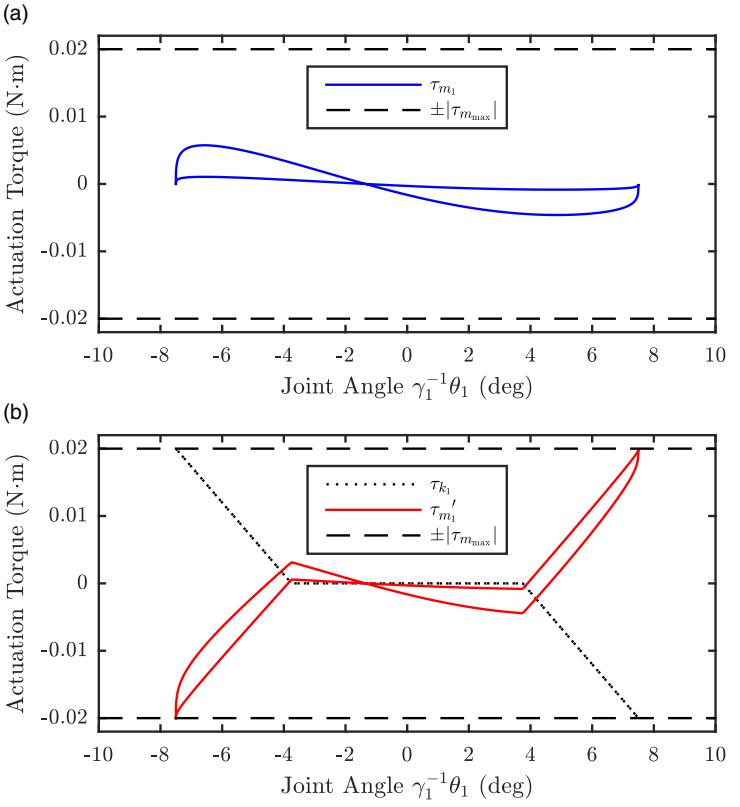


***Figure 3.*** *Waist joint torque–angle profiles for 3-DoF SA-MRR task with endpoint antagonism $\tau_k(\theta_{min})$ and $\tau_k(\theta_{max})$ changes $\tau_m'(\theta)$ only on $[\theta_{min}, \theta_{b_{min}}]$ and $[\theta_{b_{max}}, \theta_{max}]$. (a) Motor-only torque. (b) Spring torque underlaying spring-augmented motor torque. Fictitious $\pm|\tau_{m_{max}}|$ is shown near for detail clarity.*

The spring will be connected while approaching the limit angles and disconnected otherwise. This implies a position schedule of brake operation angles $\theta_{b_{\min}}$, $\theta_{b_{\max}}$ between the endpoints

$$\theta_{\min} < \theta_{b_{\min}} \leq \theta_{b_{\max}} < \theta_{\max}. \tag{11}$$

The brake state $b \in \mathbb{B}$ must change whenever either $\theta_{b_{\min}}$ or $\theta_{b_{\max}}$ is encountered, in either joint rotation sense, which is typically four times per cycle.

To satisfy $\tau_m'(\theta_{\min})$ and $\tau_m'(\theta_{\max})$ thresholds, (9)–(10) requires antagonistic spring torque (see Fig. 3) with endpoint magnitudes defined by the task, motor, and spring parameters

$$\tau_k(\theta_{\min}) = -k_s\left(\theta_{\min} - \theta_{b_{\min}}\right) = \tau_m(\theta_{\min}) + |\tau_{m_{\max}}|, \tag{12}$$

$$\tau_k(\theta_{\max}) = -k_s\left(\theta_{\max} - \theta_{b_{\max}}\right) = \tau_m(\theta_{\max}) - |\tau_{m_{\max}}|. \tag{13}$$

Selecting spring stiffness $k_s$ as design parameter fully defines both brake operation angles $\theta_{b_{\min}}$ and $\theta_{b_{\max}}$ for a task

$$\theta_{b_{\min}} = \theta_{\min} + \frac{\tau_m(\theta_{\min}) + |\tau_{m_{\max}}|}{k_s}, \tag{14}$$

$$\theta_{b_{\max}} = \theta_{\max} + \frac{\tau_m(\theta_{\max}) - |\tau_{m_{\max}}|}{k_s}. \tag{15}$$

https://doi.org/10.1017/S0263574722001060 Published online by Cambridge University Press

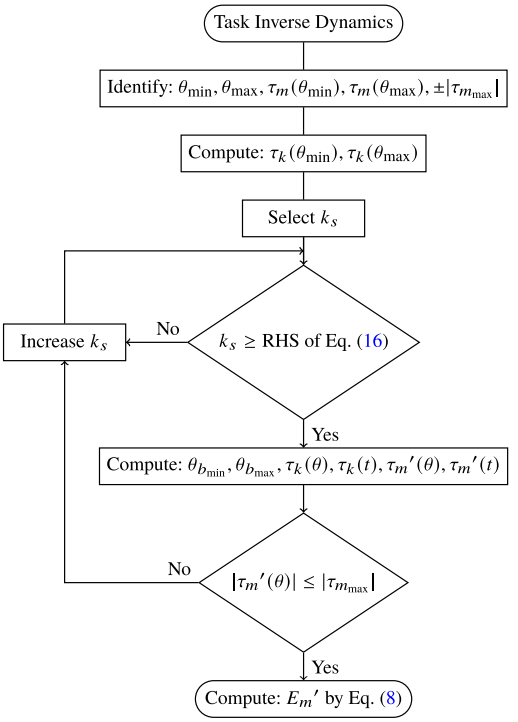


***Figure 4.*** *Flowchart illustration of the proposed endpoint safeguarding method.*

Furthermore, the task itself places an ultimate lower bound

$$k_s \geq \frac{\tau_m(\theta_{\min}) - \tau_m(\theta_{\max}) + 2|\tau_{m_{\max}}|}{\theta_{\max} - \theta_{\min}} \tag{16}$$

while theoretically $k_s$ has no task-specific upper bound.

For every potential selection of $k_s$ and its prescribed brake operation cycle (angles), physical feasibility must be verified by ensuring $|\tau_m'(\theta)| = |\tau_{m_{\max}}|$ only at $\theta_{\min}$ and $\theta_{\max}$ and that $|\tau_m'(\theta)|$ is sufficiently less than $|\tau_{m_{\max}}|$ everywhere else.

Features of the task-specific torque–angle profile may disqualify a candidate task from straightforwardly applying this antagonistic safety method to safeguard task-specific endpoint limit angles (Fig. 4). The first and most basic requirement of this method is for a unique torque value to exist at each endpoint limit angle, $\theta_{\min}, \theta_{\max}$. Neither standing still at endpoints nor precisely repeating a task will visibly change its torque–angle profile, and so both may be acceptable task features of this method. However, two task features which generally result in nonunique torque include adding or removing payload at either endpoint, and also if other robot joints have nonzero velocity while one joint is stationary at a limit. This list of task conditions and exclusions has not been exhaustively verified, but adherence to it should enable straightforward spring design and limit safeguarding no matter the SA-MRR structural configuration. Indeed, this list excludes many tasks from applying the MWM safeguarding method.

Energy consumption properties of this MWM safety method as illustrated in Fig. 4 are related strongly to torque characteristics of the task, motor, and spring. It should be noticed that the primary intent of this safety method is not to save energy. In fact, only some tasks and some design conditions can save energy as a byproduct of this method. Poor design can lead to energy increase for every task, even if the task is one which may allow energy savings by appropriate energy-aware design. Since $|\tau_m'(\theta)| > |\tau_m(\theta)|$ at $\theta_{\min}$ and $\theta_{\max}$ irrespective of $k_s$, it is true for every SA-MRR joint that the active motor energy to stand still at endpoints is always higher with this safeguarding strategy than without it. While joints

https://doi.org/10.1017/S0263574722001060 Published online by Cambridge University Press

are in motion, the cumulative motor energy increases or decreases over the time domain movements on $[\theta_{\min}, \theta_{b_{\min}}]$ and $[\theta_{b_{\max}}, \theta_{\max}]$. The extent of energy losses or savings for every task is known only by (8) after spring augmentation design and is impossible to judge from inspecting the torque–angle profile alone. In favorable tasks, energy savings may be realized by the following guidelines for spring design and SA-MRR module selection. When task-specific energy savings are possible, it is usually greatest when $|\tau_{m_{\max}}|$ minimally exceeds $\max\{|\tau_m(\theta)|\}$. This suggests choosing the smallest SA-MRR joint module and actuator possible for the task if energy is a large concern. Also when energy savings is possible, ($E'_m < E_m$), the energy-optimal $k_s$ is often identically the lowest by (16), or the smallest feasible stiffness exceeding it. Logically, a spring stiffness also exists for which endpoint safeguarding is theoretically net energetically neutral ($E'_m = E_m$), but feasibility is not guaranteed in general and must be tested. For tasks where energy necessarily increases ($E'_m > E_m$), $E'_m$ decreases to a task-specific asymptotic minimum as the design specification of $k_s$ approaches infinity (for all actuator sizes).

Nearly any spring with satisfactory $k_s$ may be used for endpoint limit safeguarding. A spring already installed in any SA-MRR joint module is suitable for any variety of tasks for which the method of Fig. 4 flows directly from start to end terminal nodes without looping. Safety in many tasks is a higher priority than energy optimality. As such, the SA-MRR may seamlessly apply this MWM safety strategy to multiple tasks simply by reconfiguring the brake operation schedule of (11) online for each new task definition. In this way, the spring installed in each SA-MRR joint may be used across several safe manipulation task scenarios or used for other applications such as the following energy-saving MWM strategy.

### *3.2. Spring assistance for energy efficiency*

The second spring-assisted MWM strategy is proposed to minimize motor energy per cycle during tasks confined for safety to small task-specific regions of the SA-MRR work envelope. The objective is to augment each task-specific torque–angle profile with the most energy-complementary spring characteristic by optimization methods, while also considering task-specific spatial safety constraints.

Augmenting motor torque with the torque characteristic of a linear spring allows design optimization of up to two parameters: stiffness $k_s$ and rest angle $\theta_0$. Intuitively, $\tau_k$ contributes to energy savings in confined regions largely by compensating gravity. Spring stiffness relates to the magnitude of $\tau_k$ over its task motion range. But $\theta_0$ biases $\tau_k$ direction sense, and so $\theta_0$ is more critical for energy-minimizing designs. Advantageously, the SA-MRR allows online repositioning of $\theta_0$ for greatest reconfigurability.

Defining optimal $\theta_0$ also relates to segregation safety. To set (or reset) $\theta_0$ initially at SA-MRR modules requires advancing the joint angle to engage the brake at $\theta_b = \theta_0$ before a task commences. Practically, then, the $\theta_0$ search space $[\underline{\theta}, \overline{\theta}]$ depends on whether the task safety constraints allow any joint to move outside the task limits $[\theta_{\min}, \theta_{\max}]$ at the outset. If so, a spatial safety analysis determines $[\underline{\theta}, \overline{\theta}]$.

To find a fully specified, complementary spring characteristic, we formulate energy-minimizing gradient optimization problem

$$\begin{aligned} \text{minimize } & f(k_s, \theta_0) = \int_{t_0}^{t_f} P'_m(t, k_s, \theta_0)\mathrm{d}t \\ \text{with respect to } & \quad k_s, \theta_0 \\ \text{subject to } & \quad k_s \geq 0 \\ & \quad \underline{\theta} \leq \theta_0 \leq \overline{\theta} \\ & \quad t_0 \leq t \leq t_f \\ \text{and } & \quad |\tau_{m_{\max}}| > \max(|\tau'_m(t, k_s, \theta_0)|) \end{aligned} \tag{17}$$

which can be solved using Matlab's nonlinear optimization function *fmincon*. Optimization enables flexibility to tailor the design search specifically for the task-specific torque and safety conditions of each joint module and simultaneously avoids infeasible designs which violate $|\tau_{m_{\max}}|$.

https://doi.org/10.1017/S0263574722001060 Published online by Cambridge University Press

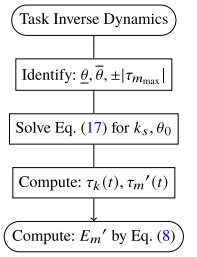


***Figure 5.*** *Flowchart illustration of the proposed energy efficiency method.*

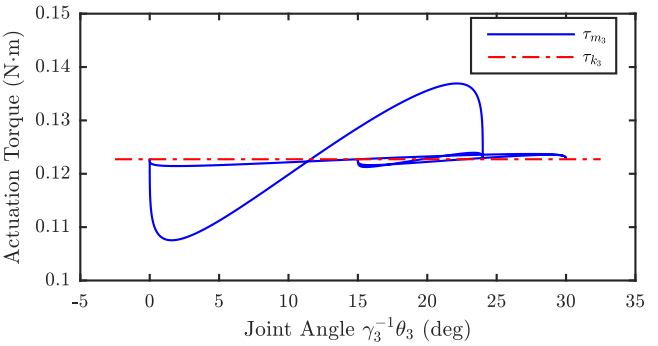


***Figure 6.*** *Elbow joint torque–angle profile (solid blue) for 3-DoF SA-MRR task with spring-assisted torque (dash-dot red) that minimizes $E_m'$ per cycle.*

This second MWM strategy and method (Fig. 5) potentially always decreases the task-specific motor energy consumption. The highest task-specific energy savings are generally achieved when both $k_s$ and $\theta_0$ are available for design (Fig. 6) compared to $\theta_0$ only. By experience, many tasks prescribe an optimized $\theta_0$ toward either the upper or lower bound of its search space, and so higher energy savings are usually possible when $\theta_0$ may be set initially outside the task boundaries, $[\theta_{\min}, \theta_{\max}]$. For joints confined for safety to $[\theta_{\min}, \theta_{\max}]$, the spring is connected the first time $\theta_0$ is reached during the task and stays connected thereafter. This has the advantage of no startup time, although energy of the first cycle typically exceeds the settled energy of each successive cycle. Clearly, the energy benefits of this MWM strategy are accentuated for tasks that repeat very often or endlessly. Experience and intuition agree that lower $k_s$ shows better reconfigurability when gravity compensation is a large portion of the actuation energy. The energy characteristics of this safety-aware MWM energy efficiency method and of the energy-aware MWM safety method are demonstrated next in a simulated manipulation task.

## 4. Simulation results

This section presents the simulation results using a 3-DoF SA-MRR manipulator model, Fig. 7(a), to demonstrate task-specific energy properties of the two MWM strategies developed for endpoint safeguarding and energy savings. Consider a positioning task similar to the procedure to loosen/tighten a 5-lug, 4.5-inch-diameter array of automotive wheel nuts in the repetitive sequence of Fig. 7(b). This task may be simplified to conform to the list of task conditions and exclusions for success as outlined in Section 3.1. The wheel is centered at [0 0.73 0.64] meters in the $x_0y_0z_0$ frame of Fig. 7(a) with all bolt axes parallel to $y_0$. The first lug is directly above the wheel center. A mean time of 2 s to advance between wheel nuts has been assumed, as well as equal, 2-s action intervals to loosen/tighten at each lug location (one cycle is 20 s). End-effector, tooling, and contact forces have not been modeled while studying the energy characteristics of the SA-MRR. Illustrations of the SA-MRR workspace envelope under the ultimate joint limits are shown in Fig. 8 compared with the apparent spring limits under the

https://doi.org/10.1017/S0263574722001060 Published online by Cambridge University Press

***Table I.*** *SA-MRR dynamic simulation parameters.*

| **Parameter** | **Module 1, 2, 3** |
|---|---|
| Gear reduction ratio, $\gamma_i$ | 100 |
| Mass of link, $m_i$ (kg) | 5 |
| Length of link, $l_i$ (m) | 0.5 |
| Distance to mass center, $l_{c_i}$ (m) | 0.25 |
| DC terminal resistance, $R_{m_i}$ ($\Omega$) | 1.5 |
| DC torque constant, $k_{\tau_i}$ (N·m/A) | 0.2 |

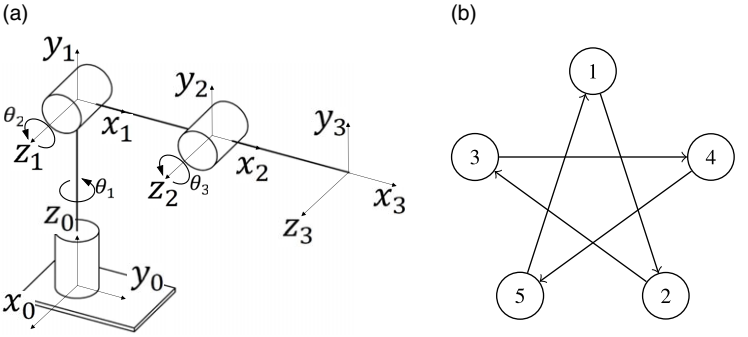


***Figure 7.*** *Simulation task and robot. (a) Shows kinematic arrangement and frame assignment of SA-MRR synthesized as 3-DoF manipulator with spring-assisted waist, shoulder, and elbow joints. (b) Illustrates the positioning sequence between wheel nuts numbered 1–5.*

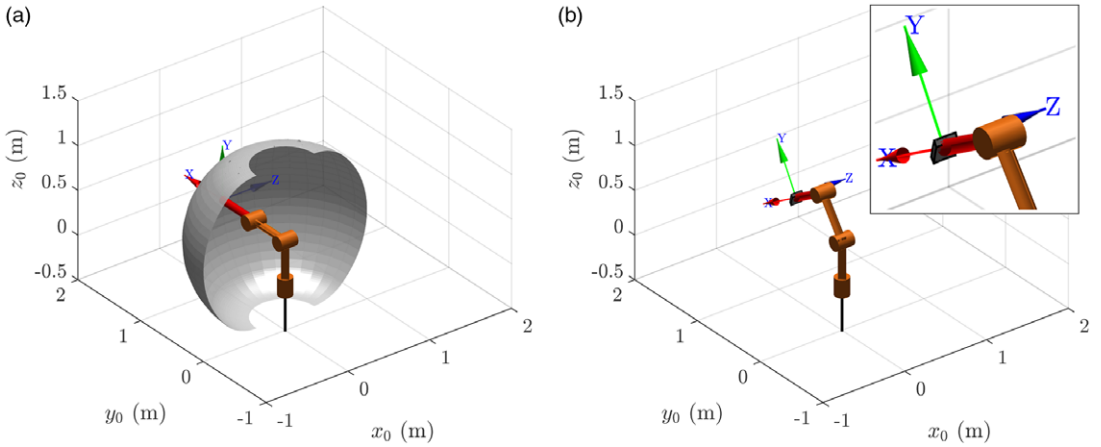


***Figure 8.*** *Illustration showing outer workspace envelope of SA-MRR for the simulated task. (a) Under the ultimate mechanical joint limits. (b) Under the proposed MWM endpoint safeguarding method, with an enlarged view of the apparent task-specific envelope as confined by the springs.*

MWM endpoint safeguarding strategy. The SA-MRR nominal dynamic parameters are given in Table I. Figure 9 shows the torque–angle profiles of all three SA-MRR joint modules for this task, as performed in the elbow-up posture.

Different MWM methods may be applied independently at SA-MRR joint modules to best suit a task. Accordingly, both MWM strategies' energy results per cycle are presented for each joint in Fig. 9 for comparison to the baseline (*Mode 1*) energy consumption. Relative energy contours of the MWM safety method are influenced primarily by the motor torque threshold and spring stiffness, Fig. 9 (middle).

https://doi.org/10.1017/S0263574722001060 Published online by Cambridge University Press

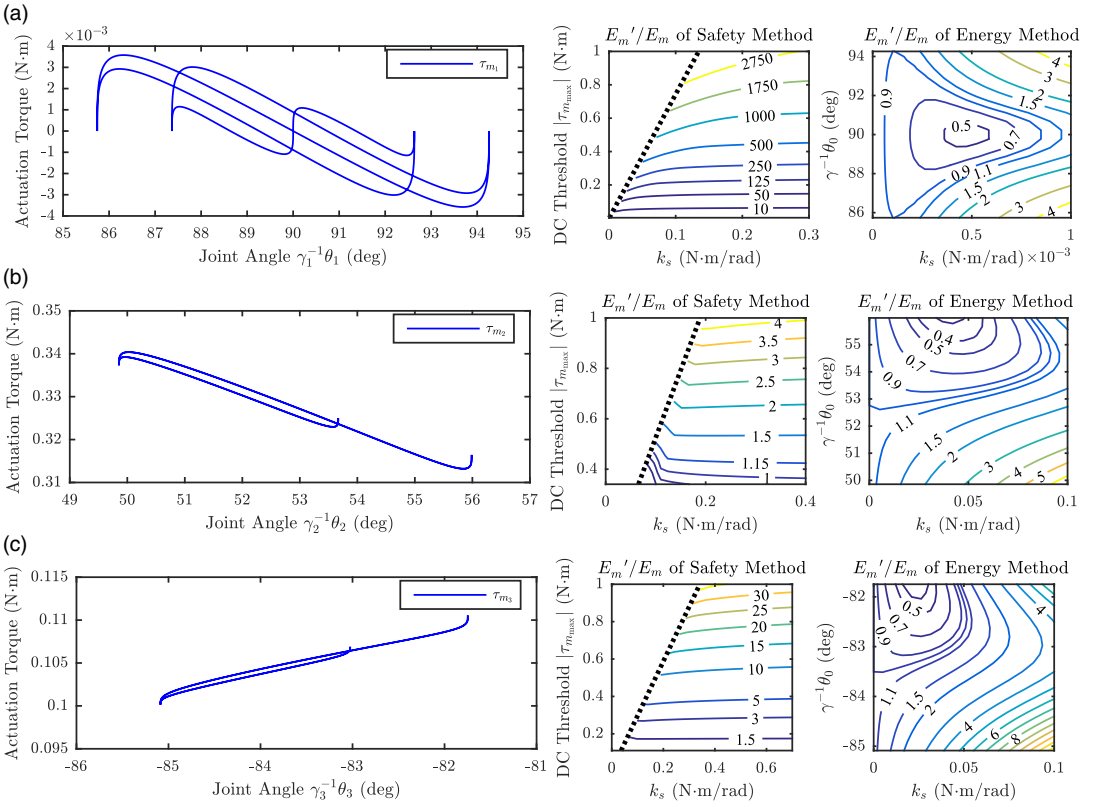


***Figure 9.*** *(Left) Task-specific torque–angle profiles of SA-MRR; (Middle) Contours of task-specific, relative energy per cycle of MWM safety method, and; (Right) Contours of task-specific, relative energy per cycle of MWM energy efficiency method for (a) Joint 1, (b) Joint 2, and (c) Joint 3. Static torque is zero throughout for Joint 1, whereas Joints 2 and 3 experience persistent gravitational torque. Each joint has unique endpoint torque. This simplified task qualifies for the MWM safety method. The MWM safety method (middle) requires the spring stiffness to exceed the lower bound (dotted) by equality to (16).*

Relative energy contours of the MWM energy method are influenced primarily by the spring stiffness and rest angle, Fig. 9 (right).

Task-specific energy of the MWM safety method is relatively insensitive to the spring stiffness design compared to the motor torque threshold, Fig. 9(a–c, middle). For this task the baseline, *(Mode 1)* energy expense $E_m$ is very low for Joint 1. As a result, adding spring antagonism to Joint 1 for safety may increase per-cycle energy $E_m'$ by a factor of tens, hundreds, or thousands, Fig. 9(a, middle). An opportunity for Joint 2 to experience energy savings with the MWM safety method is seen in Fig. 9(b, middle) with $k_s$ near 0.1 N·m/rad, and if $|\tau_{m_{\max}}|$ is near 0.4 N·m. Joint 3 shows a more moderate energy trade-off to secure the added joint limit safeguarding feature, Fig. 9(c, middle). It should be stated that half of the cycle time (i.e., 10 s) is spent stationary in this example task. This tends to decrease the potential for spring-assisted energy savings at all SA-MRR joints and for both of the proposed energy-, and safety-aware MWM strategies.

For the MWM energy efficiency strategy, an energy-optimal spring characteristic has been found (17) at each joint, for which $\theta_0$ has been restricted on the task interval $[\theta_{\min}, \theta_{\max}]$ for safety, Fig. 9(a–c, right). Energy-optimal spring design and simulated task-specific energy measures are reported in Table II and show relative savings that range between 56.8−72.6% per joint and 72.1% overall.

https://doi.org/10.1017/S0263574722001060 Published online by Cambridge University Press

***Table II.*** *Optimal spring design results and simulation energy measures.*

| | Optimal Spring Parameters | | Energy Measures (per Cycle) | | |
|---|---|---|---|---|---|
| Joint | $k_{s_i}$ (N·m/rad) | $\gamma_i^{-1}\theta_{0_i}$ (deg) | $E'_{m_i}$ (J) | $E_{m_i}$ (J) | $E'_{m_i}/E_{m_i}$ (J/J) |
| 1 | 4.69e–4 | 90.0 | 0.04 | 0.08 | 0.432 |
| 2 | 4.06e–2 | 56.0 | 25.3 | 92.3 | 0.274 |
| 3 | 2.31e–2 | −81.7 | 3.32 | 10.2 | 0.324 |
| $\sum$ | —— | —— | 28.6 | 102.6 | 0.279 |

## 5. Conclusion

In this work, two MWM methods have been developed and studied for the SA-MRR. The need for each is driven by the requirement to reduce task-specific energy consumption, improve manipulation safety, and maintain high reconfigurability. Design of each MWM strategy identified the spring characteristic and brake operation schedule that augmented the motor effort to prioritize spatial safety and minimize energy consumption. Each spring-assisted strategy works independently at SA-MRR joint modules, without modifying the original task motion trajectories. The safety-aware MWM energy efficiency method yielded overall savings of 72% in a simulated manipulation task while maintaining spatial safety constraints. We conclude this MWM energy-optimal method will very likely decrease baseline motor energy irrespective of MRR structural synthesis or (sub)optimal robot–task pairing. The energy-aware MWM safety method mechanically safeguarded the task-specific joint angle endpoints using the spring in addition to software joint limits. It should be restated that the primary intent of the energy-aware safety method is not to save energy. Accordingly, whether energy may be saved by the energy-aware MWM safety method, and to what extent, can only be known definitively from a task-by-task analysis.

In future work, we may study the MWM energy properties in a wider variety of typical tasks and conduct experimental evaluations when possible.

**Acknowledgments.** This work was supported in part by a research grant from the Natural Sciences and Engineering Research Council of Canada.

**Competing interest declaration.** The authors declare none.

**Financial support.** A research grant from the Natural Sciences and Engineering Research Council of Canada.

**Ethical considerations.** None.

**Authors' Contributions.** C. Singh and G. Liu conceived and designed this study and its methodology. C. Singh developed and investigated the proposed MWM strategies, conducted simulations and interpretation of results, and prepared this article manuscript under PhD supervision by G. Liu.

## References

[1] S. Ahmad, H. Zhang and G. Liu, "Multiple working mode control of door-opening with a mobile modular and reconfigurable robot," *IEEE/ASME Trans. Mechatron.* **18**(3), 833–844 (2013). doi: 10.1109/TMECH.2012.2191301.

[2] T. Pankov and G. Liu, "Multiple Working Mode Approach to Manipulation of Unknown Mechanisms Using A Serial Robot: A Special Case of Constrained Motion with Active and Passive Joints," **In:** *IEEE International Conference on Cyber Technology in Automation, Control, and Intelligent Systems* (2015) pp. 13–18. doi: 10.1109/CYBER.2015.7287902.

[3] V. Romanyuk, S. Soleymanpour and G. Liu, "A multiple working mode approach to robotic hammering: Analysis and experiments," *Robotica* **40**(3), 570–582 (2022). doi: 10.1017/S0263574721000680.

[4] G. Liu, Y. Liu and A. Goldenberg, "Design, analysis, and control of a spring-assisted modular and reconfigurable robot," *IEEE/ASME Trans. Mechatron.* **16**(4), 695–706 (2011). doi: 10.1109/TMECH.2010.2050895.

[5] C. Singh and G. Liu, "On Task-Specific Redundant Actuation of Spring-Assisted Modular and Reconfigurable Robot," **In:** *IEEE International Conference on Mechatronics and Automation* (2020) pp. 1191–1196. doi: 10.1109/ICMA49215.2020.9233553.
[6] M. Plooij, W. Wolfslag and M. Wisse, "Clutched elastic actuators," *IEEE/ASME Trans. Mechatron.* **22**(2), 739–750 (2017). doi: 10.1109/TMECH.2017.2657224.
[7] L. van der Spaa, W. Wolfslag and M. Wisse, "Unparameterized optimization of the spring characteristic of parallel elastic actuators," *IEEE Robot. Automat. Lett.* **4**(2), 854–861 (2019). doi: 10.1109/LRA.2019.2893425.
[8] A. Calanca and T. Verstraten, "An energy efficiency index for elastic actuators during resonant motion," *Robotica* **40**(5), 1450–1474 (2022). doi: 10.1017/S0263574721001211.
[9] N. Schmit and M. Okada, "Simultaneous Optimization of Robot Trajectory and Nonlinear Springs to Minimize Actuator Torque," **In:** *IEEE International Conference on Robotics and Automation* (2012) pp. 2806–2811. doi: 10.1109/ICRA.2012.6224621.
[10] M. Khoramshahi, A. Parsa, A. Ijspeert and M. Ahmadabadi, "Natural Dynamics Modification for Energy Efficiency: A Data-Driven Parallel Compliance Design Method," **In:** *IEEE International Conference on Robotics and Automation* (2014) pp. 2412–2417. doi: 10.1109/ICRA.2014.6907194.
[11] D. Haeufle, M. Taylor, S. Schmitt and H. Geyer, "A Clutched Parallel Elastic Actuator Concept: Towards Energy Efficient Powered Legs in Prosthetics and Robotics," **In:** *IEEE/RAS-EMBS International Conference on Biomedical Robotics and Biomechatronics (BioRob)* (2012) pp. 1614–1619. doi: 10.1109/BioRob.2012.6290722.
[12] W. Wu and P. Lin, "A Switchable Clutched Parallel Elasticity Actuator," **In:** *IEEE Internatinal Conference on Advanced Intelligent Mechatronics* (2017) pp. 1173–1178. doi: 10.1109/AIM.2017.8014177.
[13] G. Mathijssen, R. Furnémont, S. Beckers, T. Verstraten, D. Lefeber and B. Vanderborght, "Cylindrical Cam Mechanism for Unlimited Subsequent Spring Recruitment in Series-Parallel Elastic Actuators," **In:** *IEEE International Conference on Robotics and Automation* (2015) pp. 857–862. doi: 10.1109/ICRA.2015.7139278.
[14] R. Nasiri, M. Khoramshahi, M. Shushtari and M. Ahmadabadi, "Adaptation in variable parallel compliance: towards energy efficiency in cyclic tasks," *IEEE/ASME Trans. Mechatron.* **22**(2), 1059–1070 (2017). doi: 10.1109/TMECH.2016.2637826.
[15] M. Uemura, H. Goya and S. Kawamura, "Motion control with stiffness adaptation for torque minimization in multijoint robots," *IEEE Trans. Robot.* **30**(2), 352–364 (2014). doi: 10.1109/TRO.2013.2283927.
[16] M. Plooij, M. Wisse and H. Vallery, "Reducing the energy consumption of robots using the bidirectional clutched parallel elastic actuator," *IEEE Trans. Robot.* **32**(6), 1512–1523 (2016). doi: 10.1109/TRO.2016.2604496.
[17] J. Geeroms, L. Flynn, V. Ducastel, B. Vanderborght and D. Lefeber, "On the Use of (Lockable) Parallel Elasticity in Active Prosthetic Ankles," **In:** *IEEE/RSJ International Conference on Intelligent Robots and Systems (IROS)* (2020) pp. 3383–3388. doi: 10.1109/IROS45743.2020.9341679.
[18] M. Plooij and M. Wisse, "A Novel Spring Mechanism to Reduce Energy Consumption of Robotic Arms," **In:** *IEEE/RSJ International Conference on Intelligent Robots and Systems (IROS)* (2012) pp. 2901–2908. doi: 10.1109/IROS.2012.6385488.
[19] W. Brown and A. Ulsoy, "Robust design of passive assist devices for multi-dof robotic manipulator arms," *Robotica* **35**(11), 2238–2255 (2017). doi: 10.1017/S0263574716000850.
[20] M. Shushtari, R. Nasiri, M. Yazdanpanah and M. Ahmadabadi, "Compliance and frequency optimization for energy efficiency in cyclic tasks," *Robotica* **35**(12), 2363–2380 (2017). doi: 10.1017/S0263574717000030.
[21] W. Brown, Maneuver Based Design of Passive Assist Devices for Active Joints, Ph.D. dissertation, Dept. Mech. Eng., Univ. Michigan, Ann Arbor, USA, 2013.
[22] S. Bowyer, B. Davies, F. Rodriguez y Baena, "Active constraints/virtual fixtures: A survey," *IEEE Trans. Robot.* **30**(1), 138–157 (2014). doi: 10.1109/TRO.2013.2283410.
[23] X. Liu, A. Rossi and L. Poulakakis, "A switchable parallel elastic actuator and its application to leg design for running robots," *IEEE/ASME Trans. Mechatron.* **23**(6), 2681–2692 (2018). doi: 10.1109/TMECH.2018.2871670.
[24] A. Mazumdar, S. Spencer, C. Hobart, J. Salton, M. Quigley, T. Wu, S. Bertrand, J. Pratt and S. Buerger, "Parallel elastic elements improve energy efficiency on the STEPPR bipedal walking robot," *IEEE/ASME Trans. Mechatron.* **22**(2), 898–908 (2017). doi: 10.1109/TMECH.2016.2631170.
[25] T. Niehues, P. Rao and A. Deshpande, "Compliance in parallel to actuators for improving stability of robotic hands during grasping and manipulation," *Int. J. Robot. Res.* **34**(3), 256–269 (2015). doi: 10.1177/0278364914558016.
[26] W. Brown and A. Ulsoy, "Robust Maneuver based Design of Passive-Assist Devices for Augmenting Robotic Manipulator Joints," **In:** *ASME Dynamic Systems and Control Conference* (2013) pp. 1–9. doi: 10.1115/DSCC2013-3819.
[27] T. Verstraten, R. Furnémont, G. Mathijssen, B. Vanderborght and D. Lefeber, "Energy consumption of geared dc motors in dynamic applications: comparing modeling approaches," *IEEE Robot. Automat. Lett.* **1**(1), 524–530 (2016). doi: 10.1109/LRA.2016.2517820.
[28] H. Patel, C. Singh and G. Liu, "Safe Robot Operation Alongside Humans Using Spring-Assisted Modular and Reconfigurable Robot," **In:** *IEEE International Conference on Mechatronics and Automation* (2017) pp. 787–792. doi: 10.1109/ICMA.2017.8015916.
[29] P. Corke, "Robot manipulator capability in MATLAB: A tutorial on using the robotics system toolbox [tutorial]," *IEEE Robot. & Automat. Mag.* **24**(3), 165–166 (2017). doi: 10.1109/MRA.2017.2718418.

**Cite this article:** C. Singh and G. Liu (2022). "Energy-aware redundant actuation for safe spring-assisted modular and reconfigurable robot", Robotica **40**, 4498–4511. https://doi.org/10.1017/S0263574722001060